Half-metallic antiferromagnetism in $Cr_{2+x}Se$ ($0 \leqslant x \leqslant 1$): A first-principles study

I. Galanakis*
Department of Materials Science, School of Natural Sciences, University of Patras, GR-26504 Patra, Greece

K. Özdoğan†
Department of Physics, Yildiz Technical University, 34210 İstanbul, Turkey

E. Şaşıoğlu‡
Peter Grünberg Institut and Institute for Advanced Simulation, Forschungszentrum Jülich and JARA, 52425 Jülich, Germany and Department of Physics, Fatih University, 34500, Büyükçekmece, İstanbul, Turkey

(Received 10 August 2012; published 26 October 2012)

We study the behavior of the $Cr_{2+x}Se$ alloys based on state-of-the-art first-principles electronic structure calculations. We show that these alloys are of special interest since they combine possible applications in spintronics devices with a series of diverse magnetic phenomena. First, we show that Cr_2Se prefers the $C1_b$ structure while Cr_3Se crystallizes in the $D0_3$ lattice. Our calculations suggest that as we dope Cr_2Se with Cr atoms and move towards Cr_3Se, all alloys are half-metallic fully compensated ferrimagnets (also known as half-metallic antiferromagnets) with a gap in the spin-down band. All alloys follow a generalized version of the Slater-Pauling rule for the Heusler compounds and we show that for Cr_3Se a small deviation occurs due to the antibonding single band created by the 4*s* states of the Cr and Se atoms in the spin-down band structure which crosses the Fermi level. In the case of Cr_3Se we observe a metamagnetic behavior under hydrostatic pressure since Cr atoms with different symmetry present both itinerant and localized magnetic properties. Finally, calculations based on the frozen-magnon approximation reveal that the strong intersublattice antiferromagnetic coupling between the nearest-neighboring Cr atoms stabilizes the ferrimagnetic character of both Cr_2Se and Cr_3Se and leads to estimated Curie temperature exceeding considerably the room temperature. Combination of this feature together with the half-metallic antiferromagnetism makes the $Cr_{2+x}Se$ alloys ideal for realistic spintronics applications.

DOI: 10.1103/PhysRevB.86.134427 PACS number(s): 75.50.Cc, 75.30.Et, 71.15.Mb

I. INTRODUCTION

Half-metallic alloys have been widely studied due to their potential applications in spintronics.[1,2] Especially half-metallic Heusler compounds having the formula *XYZ* (known as semi- or half-Heuslers) or X_2YZ (known as full Heuslers), where *X* and *Y* are transition-metal atoms and *Z* an *sp* element, attracted intense interest since (i) most of them present very high Curie temperatures, (ii) they crystallize in a cubic high-symmetry structure closely related to the zinc blende of semiconductors, and (iii) simply by varying in the periodic table the valence of *X*, *Y*, and *Z* in a continuous way new Heusler alloys with novel properties emerge.[3,4] Galanakis and collaborators have elucidated the origin of the gap in these alloys and have shown that the total spin-magnetic moments exhibit a Slater-Pauling behavior being per unit cell in μ_B the total number of valence electrons minus 18 in the case of semi-Heuslers[5] and minus 24 in the case of full Heuslers.[6]

A special case for applications are the compounds made up from magnetic elements with exactly 18 (in the case of semi-Heuslers) or 24 (in the case of full Heuslers) valence electrons which should have a total zero spin magnetic moment in the case of half-metallicity. These alloys should be of special interest for applications since they create no external stray fields and thus exhibit minimal energy losses.[7] In literature they are named either half-metallic fully compensated ferrimagnets (HM-FCF)[8] or half-metallic antiferromagnets, which was the initial term used by van Leuken and de Groot when studying the semi-Heusler compound CrMnSb in 1995.[9] The HM-FCF character of CrMnSb has been also confirmed by calculations made by Shaughnessy and collaborators.[10] Contrary to conventional antiferromagnets here the compensation of the spin magnetic moments stems from different magnetic sublattices; e.g., in CrMnSb Cr and Mn atoms have antiparallel spin magnetic moments of about the same magnitude.[9] However, in contrast to a zero-temperature limit in which the total magnetization vanishes, at finite temperatures spin fluctuations induce a net magnetization in HM-FCFs leading to a ferrimagnetic state.[11] Except the semi-Heusler CrMnSb, also full-Heusler alloys with 24 valence electrons have been predicted to be HM-FCFs including the Mn_3Ga,[8,12,13] Cr_2MnZ (Z = P, As, Sb, Bi) alloys,[14–16] the Co-doped Mn_2VZ (Z = Al, Si) half-metallic ferrimagnetic alloys,[17] and the Cr-doped Co_2CrAl.[18] Heusler compounds are not the only family of alloys where the half-metallic anitferromagnetism has been predicted. Potential HM-FCF candidates include also the double perovskites,[19–23] superlattice structures,[24,25] diluted magnetic semicondutors,[26,27] and even Fe-based superconductors.[28]

A special case of interest would be full-Heusler compounds where *X* and *Y* are of the same chemical species. This may lead to an easier growth of these materials and thus to enhanced properties of devices based on them. Moreover in this case we would also avoid the degradation of the magnetic properties caused by impurities and atomic swaps when the *X* and *Y* are of different chemical species like in Co_2MnSi.[29] The cubic structure which results when *X* and *Y* are the same in full Heuslers is known as the $D0_3$ structure. We mentioned in the above paragraph that Mn_3Ga which has 24 valence electrons

has been predicted to be a half-metallic antiferromagnet.[8] Several experiments have been lately devoted to the growth of high-quality samples of Mn_3Ga alloy.[30–32] In Ref. 33, Li *et al.* have shown that also Mn_3Al which has 24 valence electrons is a HF-FCF and when Cr was substituted for Mn, Cr_3Al was found to have a total spin-magnetic moment of $-3\mu_B$ in accordance with the Slater-Pauling rule for half-metallic Heusler compounds. Doping of Mn_3Al with vanadium leads to the loss of half metallicity.[34] In a recent publication (Ref. 35) we had studied Cr_3Se which has also 24 valence electrons and found it to be an almost half metal with an almost zero total spin magnetic moment. The Cr atoms in the unit cell were antiferromagnetically coupled giving rise to ferrimagnetic behavior and the estimated Curie temperature was as high as ∼700 K. Thus this compound is attractive for spintronics applications. Since both Cr and Se atoms have 6 valence electrons, the Cr_2Se semi-Heusler would have 18 valence electrons and thus from the Slater-Pauling rule also this compound is likely to be a HM-FCF. Thus the $Cr_{2+x}Se$ family of alloys is a rare case where we can examine the transition from a half-metallic antiferromagnetic half-Heusler to a half-metallic antiferromagnetic full-Heusler compound simply by increasing the Cr concentration. This is the main goal of the present study and it should provide more details on the physical phenomena associated with the unique magnetic properties of these compounds. Moreover, from the applications point of view, if also Cr_2Se exhibits high Curie temperature then such alloys would be ideal for applications since voids at the Cr sites would not downgrade their magnetic properties and the performance of spintronics devices based on them.

II. COMPUTATIONAL DETAILS

$Cr_{2+x}Se$ alloys crystallize in a cubic lattice similar to the one of Heusler compounds. This lattice structure can be visualized as an fcc lattice with four sites as basis along the [111] diagonal and in Fig. 1 we present the possible structures. In the case of Cr_3Se the three Cr atoms occupy the A, B, and C sites. The A and C sites are equivalent with respect to their nearest-neighbors environment since they have four B sites occupied by Cr atoms and four D sites occupied by Se atoms as nearest neighbors. The Cr atoms at the B sites

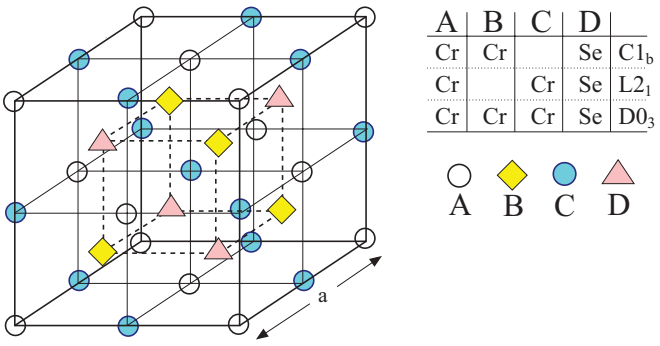

A	B	C	D	
Cr	Cr		Se	$C1_b$
Cr		Cr	Se	$L2_1$
Cr	Cr	Cr	Se	$D0_3$

A B C D

FIG. 1. (Color online) Schematic representation of the cubic structure of the various lattices adopted by the Cr-Se alloys. The cube contains exactly four unit cells.

are not equivalent with the Cr atoms at the A and C sites since the former have exclusively Cr atoms as nearest neighbors. We use the letter assigned to each site as superscript to distinguish the various Cr atoms. The lattice adopted by Cr_3Se is known as the $D0_3$ structure and it has the same symmetry operations with the fcc lattice. If now we examine the Cr_2Se alloy there are two possible arrangements for the Cr atoms: (i) They occupy the A and C sites resulting in a structure similar to the $L2_1$ structure of full-Heusler compounds (the B site is void instead of being occupied with a transition-metal atom) which belongs to the same symmetry group with the $D0_3$ structure, or (ii) they occupy the A and B sites, which are not equivalent, resulting in the $C1_b$ structure of semi- or half-Heusler alloys. The difference between the $C1_b$ and the $L2_1$-$D0_3$ structures is that for the latter ones the Cr atoms at the A and C sites occupy sites of octahedral and not tetrahedral symmetry compared to the atoms at the B and D sites (for a discussion of symmetry see Ref. 6).

We should also mention that the transition from the half-metallic ferromagnetic semi-Heusler NiMnSb crystallizing in the $C1_b$ structure to the usual ferromagnet full-Heusler Ni_2MnSb crystallizing in the $L2_1$ structure has been studied theoretically by Rusz and collaborators.[36] Also a similar transition between the half-metallic ferromagnets CoMnSb and Co_2MnSb has been studied by first-principles calculations in Ref. 37. With respect to the transition studied in this paper the magnetic and electronic properties of the end perfect compounds are different. The similarity between all three transitions stems from the fact that as we dope with X the XYZ semi-Heusler alloy and move towards the X_2YZ full-Heusler compound the magnetic and electronic properties of the intermediate alloys scale linearly with the concentration of the extra X atoms. The calculated results on the NiMnSb→Ni_2MnSb transition are in fair agreement with the experiments of Webster and Mankinar.[38]

Since the lattice constants of the perfect Cr-Se alloys are not known experimentally, we have employed the full-potential nonorthogonal local-orbital minimum-basis band structure scheme (FPLO)[39] within the generalized gradient approximation (GGA)[40] to determine the equilibrium lattice constants. We have used in all cases a dense $20 \times 20 \times 20$ **k**-mesh grid to carry out the numerical integrations. We found for Cr_3Se an equilibrium lattice constant of 5.91 Å and for Cr_2Se in the $C1_b$ structure of 5.77 Å. We have not performed calculations for Cr_2Se in the $L2_1$ structure since the latter one is not the most stable as we will discuss in the next section. To simulate the case of $Cr_{2+x}Se$ alloys with $x = 0.25$, 0.5, and 0.75 we have used a supercell containing four unit cells which is actually the cube presented in Fig. 1. We have assumed that the lattice constant varies linearly between the 5.77 and 5.91 Å of the perfect Cr_2Se and Cr_3Se alloys. We have not considered any relaxation effect since Heusler compounds and related alloys are well known to crystallize in perfect cubic structures with the atoms sitting at well-defined sites even when disorder or doping occurs.[3,4]

In Sec. III we present the electronic and magnetic properties of the perfect Cr-Se alloys and discuss the stability of each structure using total energy calculations. Since the $C1_b$ structure is found to be energetically favorable with respect to the $L2_1$ for Cr_2Se we focus on the former one in the

rest of the paper and in Sec. IV we discuss the properties of the $Cr_{2+x}Se$ family starting from the Cr_2Se ($C1_b$) alloy and moving towards the Cr_3Se one. For the latter family case we discuss the behavior of the d electrons in Sec. V and the Slater-Pauling behavior in Sec. VI. In Sec. VII we discuss the appearance of the so-called metamagnetic behavior in Cr_3Se under pressure which is related to the coexistence of localized and itinerant magnetism. In Sec. VIII we employ the augmented spherical wave method (ASW)[41] within the atomic-sphere approximation (ASA)[42] in conjunction with the GGA for the exchange-correlation potential[40] and the frozen-magnon technique[43] to determine the exchange constants and Curie temperature in the mean-field approximation (MFA). Finally in Sec. IX we summarize and conclude.

III. PROPERTIES OF THE PERFECT CUBIC ALLOYS

As we discussed above the first step of our study concerns the perfect cubic alloys. In Fig. 2 we have gathered the total density of states (DOS) and in Table I the atom-resolved and total spin magnetic moments. We will start our discussion from Cr_2Se in the $C1_b$ structure. In this case the Cr atoms at the A and B sites are nearest neighbors and due to the very small Cr^A-Cr^B distance they are antiferromagnetically coupled. As shown in the table the magnitude of their spin magnetic moments is about $2.9\mu_B$. Due to symmetry reasons Se atoms carry no net spin magnetic moments. The compounds combine the antiferromagnetic behavior with half metallicity. Although the Cr atoms at the A and B sites have spin moments of the same magnitude the different environments (Cr^A has four Cr^B and four Se atoms as nearest neighbors while Cr^B has four Cr^A and four void sites as nearest neighbors) lead to very different electronic properties and very different shape of the atom-resolved DOS (we will discuss this in detail in Sec. V). Thus instead of a usual antiferromagnet we get a fully compensated half-metallic ferrimagnet (usually also referred to as half-metallic antiferromagnet) which is much more attractive for applications.

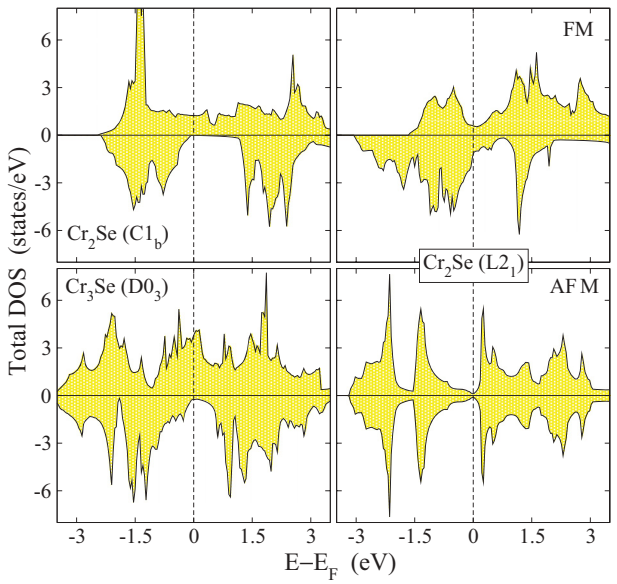

FIG. 2. (Color online) FPLO-computed DOS for all four perfect alloys under study. Note that for Cr_2Se in the $L2_1$ structure there are both a ferromagnetic and an antiferromagnetic solution. We do not present the Se-originated triple-degenerated p states which are located at around -6 to -8 eV, which carry also small Cr d admixture and the even more deeply in energy lying Se s-valence state. Positive DOS values correspond to the spin-up electrons and negative to the spin-down electrons. The Fermi level has been set as the zero of the energy axis.

In the case of Cr_2Se in the $L2_1$ structure we were able to converge to different stable magnetic configurations: either a ferromagnetic (FM) or an antiferromagnetic (AFM) coupling of the spin magnetic moments of the Cr atoms at the A and C sites. Since the Cr^A and Cr^C atoms are equivalent in the AFM case we get a classical antiferromagnet as manifested by the DOS presented in Fig. 2 and the DOS of the one Cr atom is a mirror of the DOS of the other. The Fermi level falls in a narrow region of small DOS values just below a sharp peak. In the FM case we get a classical ferromagnet which shows no half metallicity and the spin polarization at the Fermi level, as shown in Table I, is only -35% meaning that almost two-thirds of the electronic charge at the Fermi level is of spin-down character (the spin polarization is defined as $P = \frac{N^{\uparrow}-N^{\downarrow}}{N^{\uparrow}+N^{\downarrow}}$ where N represent the DOS at the Fermi level of the corresponding spin direction). Interestingly the AFM configuration is energetically more stable than the FM one by about 0.35 eV. If we dope Cr_2Se and study the $Cr_{2+x}Se$ already for $x = 0.25$ the FM configuration becomes more stable by 0.07 eV/f.u. (formula unit) while for larger values of x we were not able to converge to an antiferromagnetic coupling between the Cr atoms at the A and C sites. It seems that the occurrence of the extra Cr atoms at the B site stabilizes the ferromagnetic coupling between the Cr^A and Cr^C ones which are both antiferromagnetically coupled to the Cr^B atoms.

Overall as manifested by the energy difference values presented in Table I Cr_2Se prefers the $C1_b$ structure which is more stable than the AFM $L2_1$ by about 0.39 eV which is a considerably large energy value. The family arising by doping the C site with Cr atoms in the $C1_b$ structure stays energetically preferable to the family arising by doping the B site at the $L2_1$ structure even for $x = 0.75$. Thus we will concentrate our study on the first case. This is also the most interesting one since as shown in Table I the spin polarization remains extremely high in this family of Cr-Se starting from 100% for the Cr_2Se ($C1_b$) alloy and being as high as 88% for Cr_3Se; the positive sign reflects that at the Fermi level the gap or pseudo-gap is located at the spin-down band (we do not use the term majority and minority spin band since the compounds have zero total spin moments and thus equal amount of charge in both spin directions).

IV. THE $Cr_{2+x}Se$ FAMILY

As we discussed above the most interesting case is the family of alloys, when we use as starting point Cr_2Se in the $C1_b$ structure, since it is energetically preferable to the $L2_1$. Using a cubic supercell containing 4 unit cells we start replacing the void C sites with Cr atoms and in Fig. 3 we present the total DOS scaled per formula unit. In the energy window which we use we do not include the states rising from the Se 4s states which are very deep in energy (about 14–16 eV below

TABLE I. FPLO-computed atom-resolved spin magnetic moments in μ_B for all alloys under study. Alloys arising from doping Cr_2Se in the $C1_b$ structure are favorable in energy with respect to the ones which originated from Cr_2Se in the $L2_1$ structure; we define ΔE as the difference in total energy between the two structures ($\Delta E = E^{C1_b}_{\text{total}} - E^{L2_1}_{\text{total}}$) given per formula unit. The spin polarization at the Fermi level P is defined as $P = \frac{N^{\uparrow} - N^{\downarrow}}{N^{\uparrow} + N^{\downarrow}}$ where N represents the DOS at the Fermi level of the corresponding spin direction. In the case of Cr^A in the $C1_b$ structure there are two inequivalent sites in the 2×2 supercell used for the calculations. The first column refers to the Cr^A sites which belong to the same unit cell with the void C sites and the second column to the Cr^A sites at the same unit cell with the Cr^C atoms. With $m^{\text{f.u.}}$ we denote the total spin magnetic moment of the formula unit which is the total one of the supercell divided by the number of unit cells (there are 4 unit cells per cubic supercell as presented in Fig. 1). Finally we should note that for the perfect Cr_2Se in the $L2_1$ structure the minimum energy corresponds to an antiferromagnetic solution (Cr atoms at the A and C sites have antiparallel spin magnetic moments) but already for $x = 0.25$ this solution becomes less favorable than the ferromagnetic solution and for $x = 0.5$ we were able to converge only to a ferromagnetic solution with respect to the Cr^A and Cr^C spin moments.

			$Cr_2Se(C1_b) \rightarrow Cr_2Se(D0_3)$						$Cr_2Se(L2_1) \rightarrow Cr_2Se(D0_3)$					
	a (Å)	ΔE (eV)	P (%)	m^{Cr^A}		m^{Cr^B}	m^{Cr^C}	m^{Se}	$m^{\text{f.u.}}$	P (%)	m^{Cr^A}	m^{Cr^B}	m^{Cr^C}	m^{Se}	$m^{\text{f.u.}}$
Cr_2Se	5.77	−0.74	100%	−2.91		2.91		∼0	∼0	−35%	−2.53		−2.53	0.19	−4.87
		−0.39								0%	−3.71		3.71		0
$Cr_{2.25}Se$	5.805	−0.56	92%	−2.38	2.99	2.97	−2.06	0.05	−0.03	45%	−2.39	2.38	−2.39	0.17	−4.02
		−0.63								−17%	−3.70	1.94	3.07	−0.01	0.51
$Cr_{2.5}Se$	5.84	−0.33	89%	−1.75	−2.41	2.87	−1.89	0.07	−0.09	76%	−2.16	2.45	−2.16	0.15	−3.91
$Cr_{2.75}Se$	5.875	−0.14	89%	−1.18	−1.95	2.75	−1.65	0.08	−0.16	88%	−1.85	2.57	−1.85	0.11	−1.66
Cr_3Se	5.91		88%		−1.46	2.61	−1.46	0.10	−0.21	88%	−1.46	2.61	−1.46	0.10	−0.21

the Fermi level) nor the Se $4p$ states which are located at about 6–8 eV below the Fermi level. Doping results in more wide bands with respect to the perfect Cr_2Se alloy and as the doping increases the intensity of the DOS at the lower part of the energy window also increases. More interesting is what happens around the Fermi level. The perfect Cr_2Se is a half metal with a gap in the spin-down band. As we dope with Cr the gap starts shrinking since new states appear around the gap and when approaching perfect Cr_3Se the gap disappears and is replaced by a region of very low spin-down DOS. In the same time in the other spin direction the intensity of the DOS at the Fermi level increases with the doping and for Cr_3Se a very large value of the spin polarization is present although the spin-down gap is no more present. The states responsible for the disappearance of the gap as we will discuss in detail in the next section are the t_{1u} and e_u states which are exclusively located at the Cr atoms at the A and C sites and which obey the octahedral symmetry discussed in Sec. II and thus cannot couple with the orbitals of the Se or the Cr^B atoms.

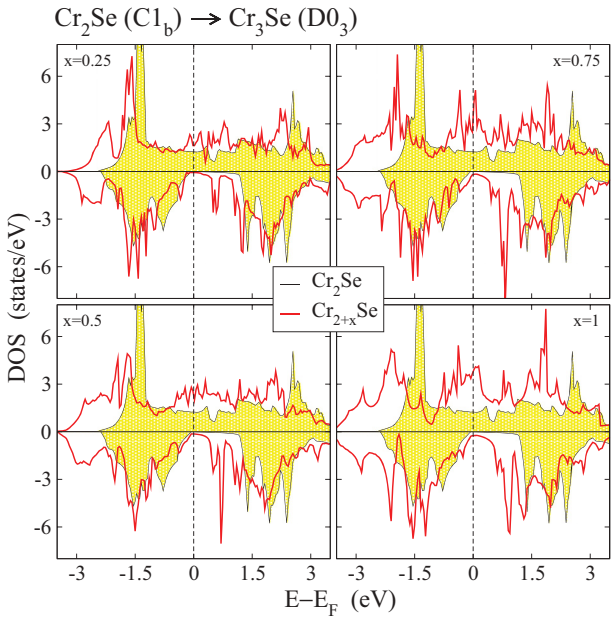

FIG. 3. (Color online) FPLO-computed total DOS for the $Cr_{2+x}Se$ alloys under study with respect to the Cr_2Se DOS. Details as in Fig. 2. Notice that all DOS have been scaled to one formula unit (see Table I).

The half metallicity in this family of alloys just discussed is also accompanied by the desirable antiferromagnetism or as it should be better described fully compensated ferrimagnetism since the total spin magnetic per formula unit presented in Table I stays close to zero for all possible values of the concentration x in $Cr_{2+x}Se$ following the Slater-Pauling behavior as discussed in Sec. VI. The supercell used for the calculations contains four unit cells and thus four C sites. If we replace one void at the C site with a Cr atom we have in the supercell three Cr_2Se ($C1_b$) and one Cr_3Se unit cells. As a result the Cr^A atoms are not all equivalent presenting variations of the spin magnetic moment which are quite important highlighting the effect of the occurrence of states obeying the octahedral symmetry as discussed in the previous paragraph. The Se and Cr^B atoms present all identical spin magnetic moments and are equivalent irrespectively of where the extra Cr atoms is situated. The doping by Cr atoms at the C site leads to a dramatic decrease of the spin magnetic moment of the Cr^A atom from about -2.9 to $-1.45\mu_B$ while the Cr^B atom keep a very large value of its spin magnetic moment of about 2.6 to $2.9\mu_B$. The difference in the behavior of the spin moments of the various Cr atoms will be elucidated in Sec. VII. In Cr_2Se both Cr atoms at the A and B sites present strongly localized magnetic moments. As we dope with Cr the C site, the Cr atoms at the A and C sites transit to itinerant magnetism while the Cr^B atom keeps the localized character of its spin magnetic moments. This allows the compounds under study to keep their fully compensated ferrimagnetic character for all values of the concentration x and the Cr^A spin moment is half

TABLE II. FPLO-computed charge density and spin density of valence states projected on selected atomic-like orbitals. The states not presented accommodate less than 0.1 electron. Deep in energy (around −15 eV) is the band with Se 4*s* character, followed by the Se 4*p* band. These bands accommodate also charge from the Cr 4*s* and t_{2g} states, respectively. The Se bands are followed by the Cr 3*d* bands which are crossed by the antibonding Se 4*s* band.

			Cr_2Se ($C1_b$)	Cr_3Se ($D0_3$)
Cr^A	4*s*	Charge	0.423	0.549
		Spin	−0.081	−0.007
	3*d*	Charge	4.974	4.932
		Spin	−2.686	−1.418
Cr^B	4*s*	Charge	0.661	0.657
		Spin	0.116	0.095
	3*d*	Charge	4.849	4.763
		Spin	2.727	2.427
Se	4*s*	Charge	1.795	1.790
		Spin	0.016	0.029
	4*p*	Charge	4.086	3.698
		Spin	0.009	0.105

in Cr_3Se what it is in Cr_2Se. Cr_3Se is an example of an alloy where itinerant and localized magnetism coexist and thus it presents the so-called metamagnetic behavior under pressure as discussed in detail in Sec. VII.

V. BEHAVIOR OF THE Cr *d* ORBITALS

In the compounds under study the crucial role is played by the Cr atoms since the role of the Se atoms is to provide bands deep in energy which accommodate *d* charge of the Cr atoms reducing the effective *d* charge of the transition-metal atoms as also occurs for the Heusler compounds.[6] In Cr_2Se both Cr atoms at the A and B sites obey the tetrahedral symmetry while in Cr_3Se the Cr atoms at the A and C sites obey the octahedral symmetry. This difference is reflected in the behavior of the *d* charge. In Table II we have gathered for all atoms the projection of the valence charge onto the atomic-like orbitals; we also present the associated spin magnetic moment defined as the difference between the charge for the spin-up electrons minus the charge of the spin-down electrons. Both Cr and Se atoms have as valence 4*s* states as free atoms. The latter are close in energy for both Cr and Se and thus create in the crystal a bonding and antibonding band each one accommodating one electron per spin direction. The bonding is mainly occupied by the 4*s* electrons of the Se atoms. Since the sum of the charge at the 4*s* states exceeds 2 electrons the surplus is accommodated by the antibonding 4*s* band which crosses the *d* states as we will discuss in the next section. The 4*p* states of Se couple strongly with the t_{2g} states of the Cr atoms which hybridize following the same symmetry operations The states coming from the 4*p* states of Se are deep in energy and accommodate in total 6 electrons. Se itself offers only 4 electrons as we can see in the table and the remaining 2 electrons come from the t_{2g} states of the Cr atoms sitting at the A and C sites which are the nearest neighbors of Se (see next section for more details).

If now we focus on the Cr *d* electrons we remark in Table II that all Cr atoms have in total almost 5 3*d* electrons one more than the free Cr atoms. This extra *d* electron in the solid comes from the 4*s* states which accommodate approximately 0.5 to 0.7 electrons in the solid. What differs among the various Cr atoms is the distribution of the *d* charge. In the tetrahedral symmetry the five *d* orbitals per spin direction can be decomposed in the double-degenerated e_g (d_{z^2} and $d_{x^2+y^2}$ orbitals) and triple-degenerated t_{2g} (d_{xy}, d_{xz} and d_{yz} orbitals) states and in Fig. 4 we present the decomposition of the *d* states on its two components. In the left panel of the figure we present the associated integrated DOS which at the end as expected reaches for both spin directions a maximum value of 2 for the e_g and 3 for the t_{2g} states. In the case of Cr^A in Cr_2Se the bands are wide and both e_g and t_{2g} states present a significant exchange splitting with very small spin-up weight below the Fermi level and very small spin-down weight above the Fermi

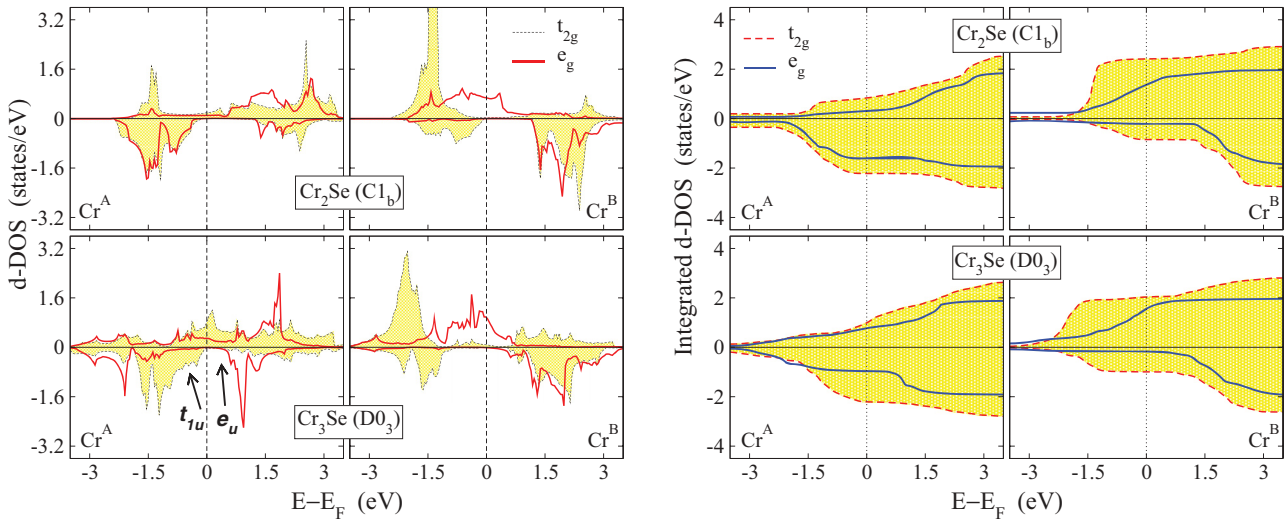

FIG. 4. (Color online) Left panel: FPLO-computed Cr *d* DOS decomposed on the triple-degenerated t_{2g} and double-degenerated e_g states for the perfect Cr-Se alloys under study. Right panel: The integrated DOS presented in the left panel. Notice that for Cr_3Se both Cr atoms at the A and C sites are equivalent. In the case of Cr_3Se we denote also the triple-degenerated t_{1u} and double-degenerated e_u states which obey the octahedral symmetry group operations and are exclusively located at the Cr^A and Cr^C sites (see text for discussion). Details as in Fig. 2.

level. Both types of d projection have a similar dispersion in energy. This behavior is also traced in the integrated DOS where up to the Fermi level we have in the spin-down direction more than 1.5 e_g electrons and more than 2 t_{2g} electrons; thus more than 3.5 out of the $\sim$5 d electrons are of spin-down character. If we move away from Cr_2Se the behavior of the d states of the $Cr^{A(C)}$ atoms changes dramatically resulting also in the halved associated spin magnetic moment shown in Table I. The change in symmetry leads to much more narrow e_g bands and the charge in these bands is almost identical for both spin directions. Moreover due to the presence of the extra Cr atom at the C site now the picture of the hybridization changes and is explained by the same reasoning as for the full-Heusler alloys in Ref. 6. We have first to consider the hybridization between the d orbitals of the Cr atoms at the A and C sites. Although these atoms are next-nearest neighbors they obey the octahedral symmetry. The hybridization of their d orbitals gives rise to bonding states which after couple to the d states of the Cr^B atom and to nonbonding states which are exclusively located at the $Cr^{A(C)}$ cites. These states are known as the double-degenerated e_u and the triple-degenerated t_{1u} states and they obey exclusively the octahedral and not the tetrahedral symmetry operations and thus they have zero weight at the Cr^B and Se sites. They are located around the Fermi level and in the right panel of Fig. 4 we denote them with arrows; notice that at the same energy region in the spin-down band the Cr^B atom has zero DOS weight. These states are also present in the spin-up band but they cannot be easily distinguished since during the projection they cannot be separated from the e_g and t_{2g} states.

Contrary to the Cr^A atom, the Cr^B atoms are less sensitive to their local environment between the Cr_2Se and Cr_3Se alloys. Their magnetism is of localized character as we will discuss in detail in Sec. VII and in the spin-up band the e_g states are well separated from the much more localized t_{2g} bands. The bands have similar dispersion above the Fermi level in the spin-down band structure. Note that for Cr^B the spin-up states are the majority ones since they are antiferromagnetically coupled to the Cr^A atoms. The Fermi level clearly crosses the e_g bands in the spin-up direction and in the spin-down band there is a large gap due to the large spin exchange splitting between the t_{2g} states. This behavior is also reflected more clearly in the integrated DOS. Up to the Fermi level, almost all 2 spin-up e_g states are populated while the spin-down e_g states are empty and thus e_g states contribute about $2\mu_B$ to the spin magnetic moment of Cr^B atoms. In the case of the t_{2g} states at the Fermi level the integrated DOS accounts for about 2 for the spin-up states and 1 for the spin-down states adding another $\sim 1\mu_B$ to the spin magnetic moment of the Cr^B atoms.

VI. BAND STRUCTURE AND SLATER-PAULING BEHAVIOR

In this section we will also discuss the band structure of the Cr_2Se and Cr_3Se alloys. Band structure calculations offer a solid background to confirm the conclusions drawn in previous sections. In Fig. 5 we present the band structure of both alloys under study presenting with solid lines the spin-down bands and with dashed lines the spin-up case. We have chosen to present only along two high-symmetry directions to make

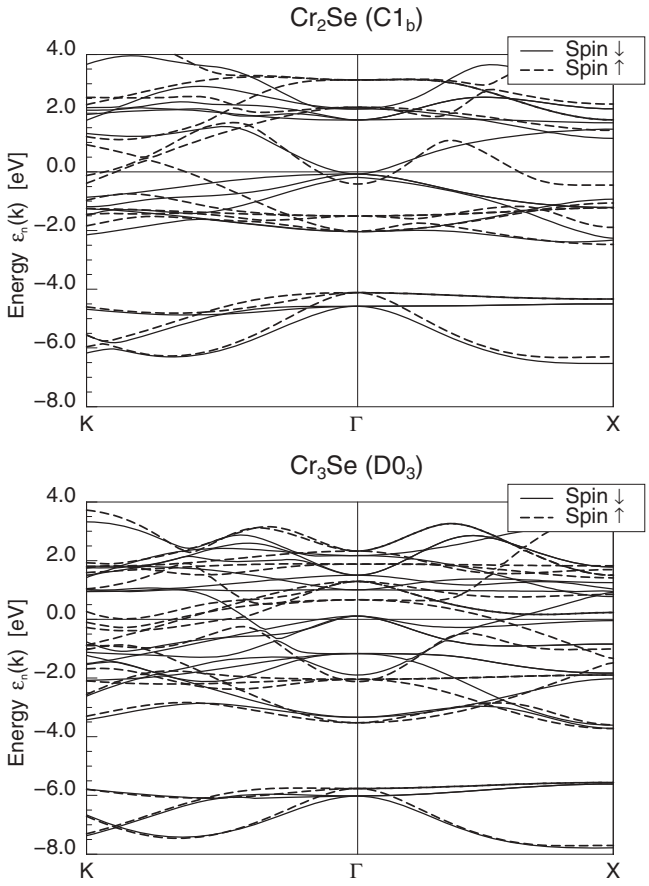

FIG. 5. FPLO-computed spin-resolved band structure of both perfect compounds under study. The zero energy has been chosen to represent the Fermi energy. The solid lines correspond to the spin-down electrons and the dashed lines to the spin-up electrons. The deep-lying Se bonding s band (coming from the Se 4s states in the free atom) at about -14 to -16 eV is not shown. The lowest shown bands are the triple-degenerated Se 4p band followed by the bonding double-degenerated Cr e_g bands and the bonding triple-degenerated Cr t_{2g} bands. In the case of the Cr_3Se spin-down band structure just below the Fermi level are the nonbonding triple-degenerated t_{1u} bands. A single band crossing the occupied 3d bands in the Cr_3Se alloy is the antibonding Se 4s band.

it more easy to understand and discuss. There is a single valence band at about -16 eV which is not presented. First for both compounds we remark a triple-degenerated band (the term degeneration refers to the behavior of the bands at the Γ point which is directly associated with their character in real space) at about -8 to -6 eV which is well separated from the other bands. On top of these bands there is a double-degenerated band and then starts a series of more complex triple-degenerated bands, especially in the case of Cr_3Se where we have more valence electrons. If we look very carefully at the band structure for Cr_3Se we can also find a single, at the Γ point, band crossing both the Fermi level and the triple-degenerated bands around it.

To make all these remarks more clear, we have drawn in Fig. 6 the Cr_3Se bands following the fat-band scheme. In this scheme the contribution of each atomic-like orbital to the band structure is revealed; the thickness of the presented fat band

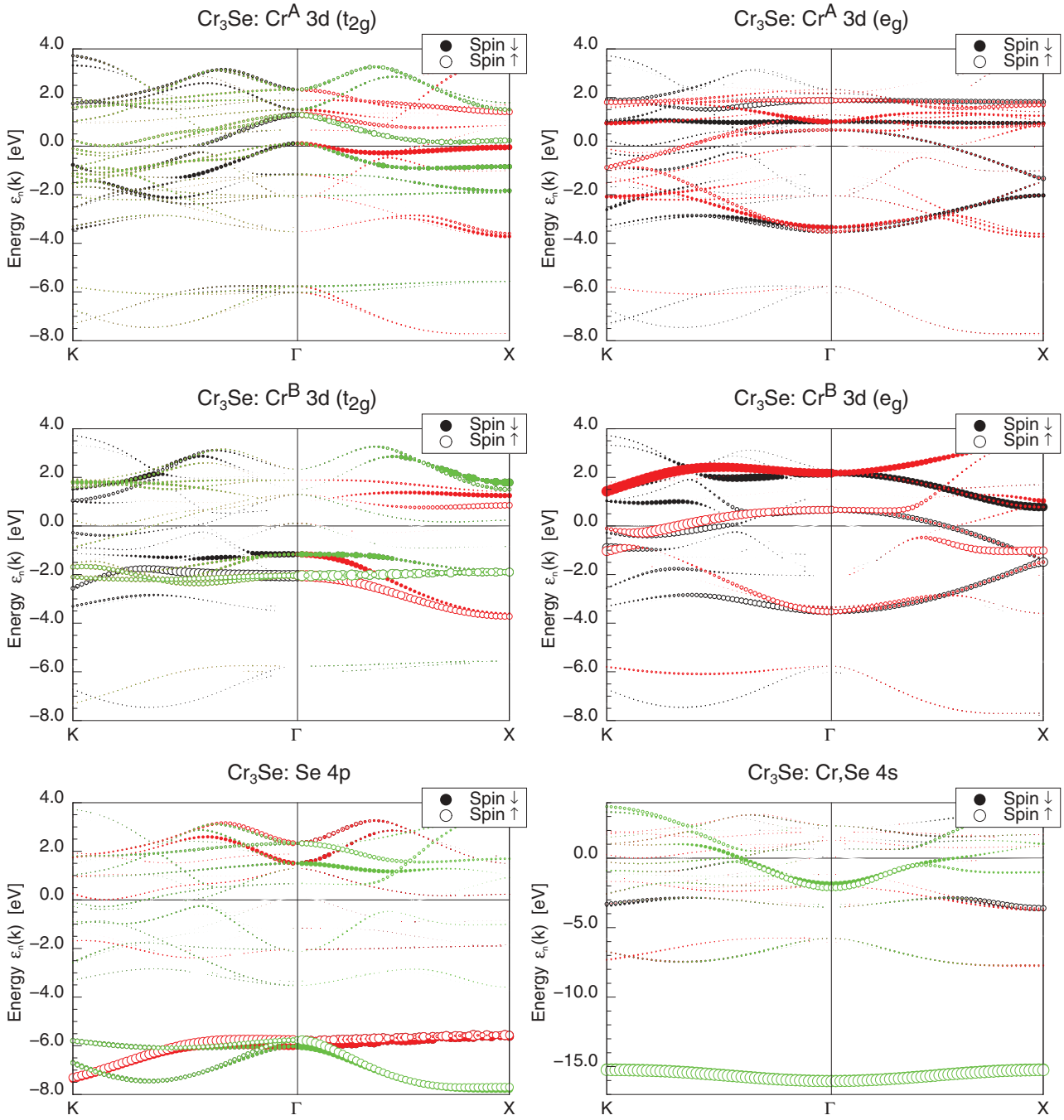

FIG. 6. (Color online) FPLO-computed atom and orbital resolved band structure of Cr_3Se alloy using the fat-bands scheme. Filled circles refer to the spin-down states and open circles to the spin-up states. In the lower left panel we present the bands originating from the 4*s* states of Se which have also a strong Cr 4*s* admixture (note that in this case also the energy bounds are different).

is proportional to the contribution of each atomic orbital to the band structure; different colors are not significant since, e.g., for the double-degenerated e_g states red and black color distinguish the two e_g states. Empty spheres refer to the spin-up states and filled spheres to the spin-down states. In the lower right panel we present the contribution of the Cr and Se 4*s* states; note that the scale in the vertical axis is different than all other presented band structures. There is an almost flat band at about −15 eV which accommodates the bonding 4*s* orbitals. For both spin directions there is a single at the Γ-point band which crosses the Fermi level and the various triple-degenerated bands around it. This single band accommodates the antibonding 4*s* states of the Cr and Se atoms and is partially filled. The triple-degenerated bands at about −8 to −6 eV originate from the Se 4*p* states as shown in the lower-left panel. These bands as discussed in the above section also contain a small admixture of $Cr^{A(C)}t_{2g}$ states as can be deduced from the top left panel where the latter fat bands are presented. The antibonding Se 4*p*–$Cr^{A(C)}$ t_{2g} bands are above the Fermi level as shown in the lower-left panel. The double-degenerated

bands following these bands in the energy axis are the ones coming from the e_g states of both the $Cr^{A(C)}$ and Cr^B atoms as revealed by the fat bands in the top- and middle-right panels. The antibonding e_g states cross the Fermi level for the spin-up direction (empty spheres) while they are entirely above the Fermi level for the spin-down direction (filled spheres) where the pseudogap exists. These bands are followed by the triple-degenerated t_{2g} bands which have their main weight at the Cr^B atoms (middle right panel). Touching the Fermi level are the spin-down t_{2g}-like states of $Cr^{A(C)}$ (top-right panel) which have vanishing weight at the Cr^B atom. These states are in reality the triple-degenerated t_{1u} states, discussed in the previous section, located exclusively at the $Cr^{A(C)}$ atoms which cannot be distinguished from the t_{2g} states in our calculations. In the case of Cr_2Se the band structure is similar with the exception that there are no t_{1u} states and the antibonding 4*s* states are above the Fermi level.

In Ref. 6 it was shown that for the full-Heusler compounds like Cr_3Se the total spin-magnetic moment M_t follows a Slater-Pauling rule being inμ_B the total number of valence electrons Z_t minus 24, reflecting the fact that there are exactly 12 occupied spin-down states. In Ref. 5 for the semi- or half-Heuslers like Cr_2Se in the $C1_b$ structure the similar Slater-Pauling rule is $M_t = Z_t - 18$. The Cr and Se atoms have both 6 valence electrons as free atoms and thus Cr_2Se and Cr_3Se have 18 and 24 valence electrons, respectively, and thus in the case of half metallicity they are expected to have zero total spin magnetic moment. In the case of Cr_2Se this is true and the spin-down band structure is similar to the spin-down band structure of semi-Heusler alloys; thus this alloy is a fully compensated half-metallic ferrimagnet. In the case of Cr_3Se there is a small deviation from the zero total spin magnetic moment as shown in Table I due to the single 4*s* band crossing the Fermi level. In the full Heuslers studied in Ref. 6 this band in the spin-down band structure was situated above the Fermi level. In the case of Cr3Se the levels of the Cr and Se 4*s* states are such that the crossing occurs and the total number of spin-down states is slightly larger than the 12 of Heusler compounds leading to a small deviation of the total spin magnetic moment of the ideal zero value and a spin polarization at the Fermi level slightly deviating from the perfect 100%. For the intermediate compounds studied in Sec. IV the hybridization is even more complex since we have different unit cells and it is meaningless to try to derive from the band structure a Slater-Pauling rule for each value of the concentration x. It is obvious since half metallicity is preserved together with an almost zero total spin magnetic moment in the formula unit that the Slater-Pauling relation just mentioned behaves with the concentration as $M_t = Z_t - (18 + 6 \times x)$ and thus for $x = 1$ we end up with the rule for the half-metallic full-Heusler compounds. This rule ensures that for any value of the concentration x the total spin magnetic moment is zero for half metallicity to occur in the Cr-Se alloys. More calculations on compounds transiting from half-metallic semi- to full Heuslers upon doping are needed to ensure the validity of this generalized Slater-Pauling rule.

Finally we should also discuss the appearance of magnetism and its connection to the lattice for both Cr_2Se and Cr_3Se alloys. The first question which rises is why magnetism appears in these alloys. We performed nonmagnetic calculations for both Cr_2Se and Cr_3Se alloys. For the Cr_3Se the DOS in the nonmagnetic case (not shown here) is of a usual metal with a large peak exactly at the Fermi level and thus due to Stoner theorem the magnetic order is preferred. In the case of Cr_2Se in the C1b structure the DOS of the nonmagnetic case (not shown) reveals a zero-band-gap semiconductor with large peaks exactly above and below the Fermi level. Thus the compound prefers to be magnetic since in the nonmagnetic case the electrons occupying the states just below the Fermi level lead to a very high total energy and the alloy prefers the magnetic order in order to lower its total energy. The second question which rises is, why does the gap appear?, and whether this is related to the structure. This point has been discussed in detail in Ref. 5 for the semi-Heusler alloys like Cr_2Se and in Ref. 6 for the full-Heusler alloys. The symmetry of the lattice in both cases dictates the hybridization of the *d* orbitals of the Cr atoms and thus the opening of the gap. Schematic representations of these *d*-*d* hybridizations for the half-metallic NiMnSb and Co_2MnGe Heusler compounds can be found in Ref. 44 and the same reasoning is valid also for the Cr_2Se and Cr_3Se compounds, respectively. Finally, from the Slater-Pauling rules we expect both Cr_2Se and Cr_3Se to have exactly zero total spin magnetic moments. To achieve this the nearest-neighboring Cr atoms should have antiparallel spin magnetic moments. This phenomenon is already known due to the work of Bethe and Slater who plotted the so-called Bethe-Slater curve.[45] The spin magnetic moments of the early transition metals like V, Cr, and Mn have the tendency to couple antiferromagnetically when the atoms are close neighbors while they couple ferromagnetically when the distance is larger. This is due to the overlap of their *d* orbitals. Several examples exist in the family of Heuslers like the Mn_2VZ alloys where the sequence of the atoms is Mn-V-Mn-*Z* and the Mn and V atoms have antiparallel spin moments,[46] and the Cr_2CoGa Heusler where Cr atoms are also nearest neighbors and couple antiferromagnetically.[47] Even in ferromagnetic compounds like Ni_2MnAl when disorder occurs and Mn atoms become closest-possible neighbors their spin moments are antiferromagnetically coupled.[48]

VII. METAMAGNETISM

An interesting phenomenon occurring in some Heusler compounds is the so-called metamagnetism. Rhee and collaborators found in the case of Fe_3Al alloys a sudden drop in the total spin magnetic from 4.6 to 4μ_B upon compression.[49] This behavior was called metamagnetism and it was explained in terms of the coexistence of itinerant and localized spin magnetic moments in Fe_3Al. The coexistence of these two types of magnetism has been also predicted for the Heusler compounds Ni_2MnSn[50] and Mn_2CoGa.[51] and thus it would be interesting to examine whether the same phenomenon occurs also in the compounds under study. The first step is to examine how the spin moments change upon compression. Starting from the equilibrium values, 5.77 Å and 5.91 Å for $Cr_2Se(C1_b)$ and Cr_3Se, respectively, we compress in a uniform way the lattice keeping the cubic symmetry of Fig. 1 and simulating the hydrostatic pressure. We present our results in Fig. 7. In the case of Cr_2Se the atomic spin moments are extremely localized. Thus they are little affected by compression (the

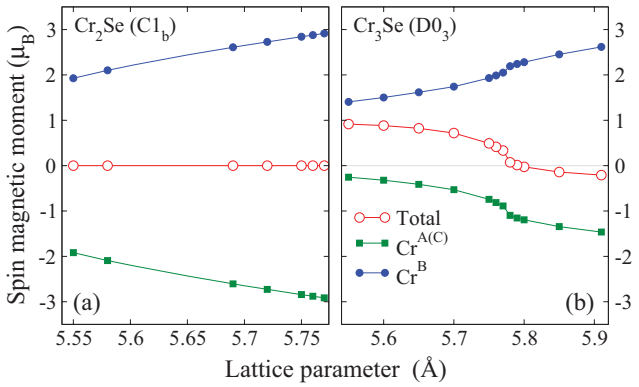

FIG. 7. (Color online) FPLO-computed behavior of the atom and total spin magnetic moments of the perfect Cr-Se alloys under hydrostatic pressure. Cr_3Se is at the verge of metamagnetism since $Cr^{A(C)}$ spin moments present an itinerant character while the Cr^B spin moment is localized.

absolute values of the Cr atomic spin moments decrease by about 30% between the two extreme lattice constants in Fig. 7). Even when we perform calculations for a lattice constant of 5.55 Å, which is a huge compression, the spin magnetic moments have a magnitude of about $2\mu_B$ and the total spin magnetic stays always equal to zero.

The case of Cr_3Se is completely different. When we reach 5.77 Å the atomic spin moments show a sudden drop in their magnitude a clear sign of metamagnetic behavior. Moreover the spin moments of the Cr atoms at the A and C sites drop fast approaching the zero value. The Cr^B atoms show an opposite behavior and keep a pretty large value (again between the two extreme lattice constants in Fig. 7 the Cr^B spin moment drops by approximately 30%). As a result below the threshold of 5.77 Å the Cr^B dominates the system and the total spin magnetic moment starts deviating from the zero spin magnetic approaching the value of the Cr atom at the B site. A plausible explanation is that the Cr atom at the B site shows a strongly localized spin magnetic moment which is less affected by compression. On the contrary the Cr atoms at the A and C sites are strongly hybridized although second neighbors due to the fact that they obey the octahedral and not the tetrahedral symmetry as explained in previous sections. The Cr atoms at these two sites present spin magnetic moments with a strong itinerant character and as we compress the lattice we lead to a strong hybridization effect and thus to vanishing spin magnetic moments at the A and C sites.

To confirm our assumption we have drawn in Fig. 8 the charge and spin density plots on the [110] plane. We have chosen this plane since as shown in the top panel all four atoms for Cr_3Se are present. If we look at the charge density presented in the middle panel we see no surprises. Most of the space is filled with dark blue color which corresponds to vanishing charge density and around the position of the atoms we have small circles of light blue where the valence charge is concentrated. Much more interesting is the spin density, defined as the difference between spin-up and spin-down charge, presented in the lower panel of Fig. 8. Green corresponds to zero spin density. If we compare the spin density plot with the atom position in the upper panel we

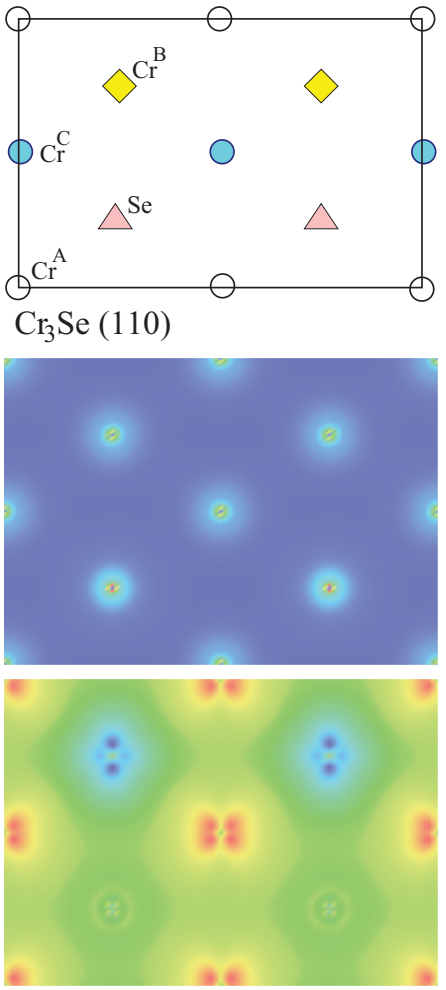

FIG. 8. (Color online) Upper panel: Schematic representation of the (110) plane of the Cr_3Se alloy. Middle panel: Distribution of the total charge density for the plane shown in the upper panel; brighter colors correspond to large intensity and deep blue to the almost constant charge density in the interstitial region. Lower panel: Distribution of the spin density defined as the charge density for the spin-up electrons minus the charge density for the spin-down electrons; blue corresponds to the maximum positive spin density, red to the maximum negative spin density, and the green color to the zero spin density.

see that the spin density around the Se atoms is very small reflecting the very small spin moments in Table I. Around the Cr^B atoms we have a small ellipse of blue color which corresponds to positive spin density. This spin density is localized around the Cr atoms at the B sites and is separated by a zero spin density (green color) from the other Cr atoms. If now we look at the Cr atoms at the A and C sites which are situated along chains in the [001] direction we see that around each atom we have a double red structure which is the sign of the octahedral symmetry (red means negative spin density). Along the [001] chains the $Cr^{A(C)}$ atoms are connected by regions of light green which corresponds to small values of negative spin density. Thus the Cr atoms at the A and C sites, although they are next-nearest neighbors, strongly hybridize due to the octahedral symmetry and present spin magnetic moments of strongly itinerant character which is seriously

affected by compressions. At 5.77 Å the compression increases sharply the hybridization leading to a sharp drop of the $Cr^{A(C)}$ spin magnetic moments.

Finally we should note that we have performed similar calculations also for Cr_2Se in the $L2_1$ structure presented in Secs. II and III both in the FM and AFM configurations. Although in this case both the A and C sites are occupied by the Cr atoms, the spin magnetic moments are strongly localized even in the FM case where the octahedral symmetry is easily recognized due to the double red peak similar to the shape of the spin density of $Cr^{A(C)}$ atoms in Cr_3Se. The localized character of the spin moments is such that even for large degrees of compression the spin magnetic moments stay almost identical to the values for the equilibrium lattice constant in Table I. Thus the occupancy of the B sites in Cr_3Se is crucial for the itinerant character of the spin magnetic moments of the $Cr^{A(C)}$ atoms and the latter cannot be simply explained by the octahedral symmetry of the Cr atoms at the A and C sites.

VIII. EXCHANGE CONSTANTS AND T_C

For realistic applications a crucial quantity is the Curie temperature, T_C. Ferrimagnets such as the ones under study should have T_C well above room temperature so that they exhibit significant magnetic properties at the latter temperature where devices operate. To study it we have employed the formalism presented in Ref. 52. As stated in Sec. II we employed the ASW method for the electronic structure calculation of the Cr_2Se and Cr_3Se alloys in the $C1_b$ and $D0_3$ lattice structures and then the frozen magnon approximation[43] to calculate the exchange constants and the mean-field approximation (MFA) to estimate the T_C. In Fig. 9 we present for both compounds under study the Cr intrasublattice Heisenberg exchange constants as a function of the Cr-Cr distance. As seen, the short-range behavior of the exchange constants are quite complicated due to the competing exchange mechanisms in Heusler alloys as will be discussed in detail at the end of this section.[53] But the long-range exchange constants present the expected general characteristics for the half metals; i.e., they are heavily damped due to the half-metallic gap and above three lattice constants

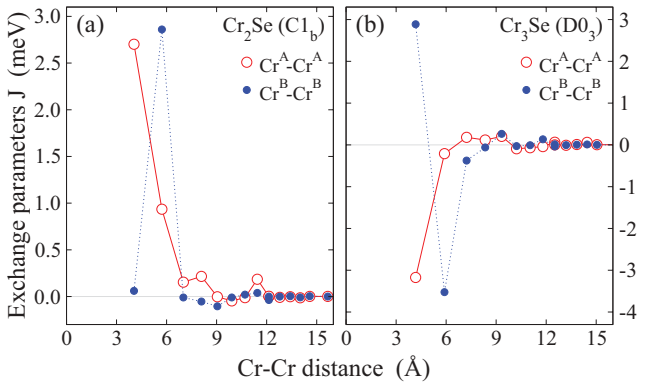

FIG. 9. (Color online) (a) ASW-based calculated intrasublattice Cr-Cr exchange constants as a function of the distance for Cr_2Se in the $C1_b$ lattice structure; (b) the same for Cr_3Se in the $D0_3$ structure.

all exchange parameters are nearly zero.[36,54–57] The Cr^B atoms in the Cr_2Se case have a vanishing exchange constant when they are the closest possible. The interaction becomes strongly magnetic for a Cr^B atom and its neighbors in the second shell and then vanishes as expected for half metals. In the case of Cr_3Se alloys the interaction between closest Cr^B atoms is positive favoring ferromagnetism and then contrary to Cr_2Se it becomes negative favoring antiferromagnetism for the second-closest Cr^B atoms. Since Cr^B atoms carry almost the same spin-magnetic moment in both compounds, it is obvious that even intrasublattice exchange interaction depends strongly on the behavior of all the sublattices.

To make our results easier to understand in Table III we present both the on-site intrasublattice and intersublattice Cr-Cr exchange constants where we have taken into account the sum of the exchange constants as the ones presented in Fig. 9 over all neighbors. We do not present the cases where the Se atoms are involved since their very small spin magnetic moments lead to vanishing exchange constants both between Se-Se atoms as well as Se-Cr atoms. In Cr_2Se the intrasublattice exchange constants between the Cr atoms at the A sites ($J_0^{A\text{-}A}$) favors their ferromagnetic coupling, which is also the case for the intrasublattice interactions between the Cr atoms at the B sites. But as we can remark the main interaction is the antiferromagnetic intersublattice interactions between the Cr atoms at the A and B sites ($J_0^{\text{A-B}}$) which is one order of magnitude larger. The Cr^A and Cr^B atoms are nearest neighbors and this large exchange constant stabilizes the antiferromagnetic coupling of their spin magnetic moments and thus the ferrimagnetic behavior of the Cr_2Se compound. This robust ferrimagnetism is also reflected on the calculated T_C which reaches 2296 K if only the A-B intersublattice interactions are taken into account and increases to 2524 K if also the A-A and B-B intrasublattice interactions are taken into account.

The case of Cr_3Se is more complex due to the presence of the third Cr sublattice. Intrasublattice interaction between the Cr atoms in the A or C sublattice favor antiferromagnetic coupling of their spin moments although a ferromagnetic one is observed in our calculations. This is due to the larger intersublattice negative exchange coupling between the Cr atoms at the B sublattice and the Cr atoms either in the A or C sublattices. Thus although ferrimagnetism is favored, it is not as robust as in the Cr_2Se case and the calculated T_C reaches a value of 770 K if only the A-B, B-C, and A-C intersublattice interactions are taken into account and it is slightly lower when also the intrasublattice interaction favoring a different magnetic order in the A and C sites are taken into account. But overall the T_C is well above the room temperature and all the compounds in the $Cr_{2+x}Se$ family are suitable for realistic applications.

Finally, we would like to dwell on the large difference between the calculated Curie temperatures of the Cr_2Se and Cr_3Se compounds. This difference can be traced back to the exchange interactions and the role of the half-metallic gap on the exchange coupling mechanisms in Heusler alloys. Extensive studies on multisublattice complex Heusler alloys have shown that there are several exchange interactions, which coexist and which are mixed together. To simplify the discussion let us write the total magnetic exchange field

TABLE III. On-site intrasublattice ($J_0^{\text{A-A}} \equiv \sum_{\mathbf{R}} J_{\mathbf{0R}}^{\text{Cr}^A-\text{Cr}^A}$, where **R** is the lattice vector) and intersublattice ($J_0^{\text{A-B}} \equiv \sum_{\mathbf{R}} J_{\mathbf{0R}}^{\text{Cr}^A-\text{Cr}^B}$) Cr-Cr exchange constants (in meV) and mean-field Curie temperatures (in K) for Cr_2Se in the $C1_b$ lattice structure and Cr_3Se in the $D0_3$ structure. Calculations are based on the ASW electronic structure method in conjunction with the frozen magnon approximation.

Compound	$J_0^{\text{A-A}}$	$J_0^{\text{B-B}}$	$J_0^{\text{C-C}}$	$J_0^{\text{A-B}}$	$J_0^{\text{A-C}}$	$J_0^{\text{B-C}}$	$T_{\text{C}}^{\text{inter}}$ (K)	$T_{\text{C}}^{\text{all}}$ (K)
Cr_2Se	43.81	14.42		−296.73			2296	2524
Cr_3Se	−31.43	10.20	−31.43	−64.49	15.51	−64.49	770	692

acting on the Cr magnetic moment at site A as $J_{\text{total}}^{A} = J_{\text{direct}}^{AB} + J_{\text{indirect}}^{AB} + J_{\text{indirect}}^{AA}$, where the first two terms represent the direct and indirect exchange couplings between Cr atoms at A and B sites. The former, i.e., the direct coupling, which is due to the overlap of the Cr 3*d* wave functions, provides the leading contribution to the total exchange coupling and determines the character of the magnetic state, while the long-range indirect part (second and third terms) is due to the coupling of the Cr 3*d* moments to the itinerant *sp* electrons, which can be separated into two contributions: $J_{\text{indirect}} = J_{\text{RKKY}} + J_{\text{S}}$. The first term is a RKKY-like ferromagnetic term which stems from the interaction between the Cr 3*d* moment and the conduction electron states inducing a spin polarization in conduction electron sea. Note that the amplitude of this polarization determines the strength of the RKKY-like exchange coupling. However, the second term has different origin; it arises from virtual-charge excitations in which electrons from local 3*d* states of the Cr atom are promoted above the Fermi sea providing an additional contribution to the indirect exchange coupling. This term depends mostly on the distance of the unoccupied total DOS (mainly Cr 3*d* peaks) from the Fermi level. The closer the peaks to the Fermi level the stronger the J_{S}. Moreover, in contrast to the first term, this second term is always antiferromagnetic and its strength decays exponentially with distance. The overall magnetic behavior depends on competition of all three terms. A detailed discussion on the exchange mechanism in multisublattice Heusler alloys can be found in Ref. 53. Returning back to Curie temperature of the present compounds the main contribution to the T_{C} is provided by the intersublattice Cr-Cr exchange interactions as seen from the Table III. From Cr_2Se to Cr_3Se the reduction of $J_0^{A\text{-}B}$ can be attributed to two factors: (i) reduction of the Cr sublattice magnetic moments from Cr_2Se to Cr_3Se since the value of the magnetic moments is absorbed into the exchange parameters in mapping the complex itinerant electron system onto the classical Heisenberg model, and (ii) substantial contribution of the antiferromagnetic exchange coupling J_{S} into the $J_0^{A\text{-}B}$, which can be seen from total DOS presented in Fig. 3, where the total DOS above the Fermi level increases with concentration x revealing an increased weight of the J_{S} contribution. This is very well reflected in intrasublattice exchange interactions presented in Fig. 9, where from Cr_2Se to Cr_3Se the Cr^A-Cr^A coupling changes sign from ferromagnetic to antiferromagnetic one and Cr^B-Cr^B shows ferromagnetic-antiferromagnetic oscillations. A similar behavior is obtained for the intrasublattice exchange interactions of the Cu-doped NiMnSb and Sb-doped AuMnSn in Refs. 58 and 59. With increasing Cu (Sb) content the $Ni_{1-x}Cu_xMnSb$ ($AuMnSn_{1-x}Sb_x$) system undergoes a phase transition from ferromagnetic to antiferromagnetic state in very good agreement with experiments.[60,61] We note that for the present systems the T_{C} is estimated within the simple mean-field approach, in which the spin fluctuations are neglected. More rigorous treatments like the random phase approximation or classical Monte Carlo methods are expected to reduce mean-field T_{C} by about 40%[52,62,63] especially for the case of Cr_2Se due to the small number of nearest-neighborhood Cr atoms compared to the Cr_3Se case, but in both cases T_{C} will stay far above room temperature.

IX. SUMMARY AND CONCLUSIONS

We have studied the behavior of the $Cr_{2+x}Se$ alloys based on state-of-the-art first-principles electronic structure calculations. These alloys are found to be of special interest since they combine possible applications in spintronics devices with a series of diverse magnetic phenomena.

First, we have shown that Cr_2Se prefers the $C1_b$ structure of semi- (also known as half-) Heusler alloys. Cr_3Se on the other hand crystallizes also in a cubic $D0_3$ structure similar to the full-Heusler alloys. As we dope Cr_2Se with Cr atoms and move towards Cr_3Se all compounds under study are half metals with a gap in the spin-down band. Moreover their total spin magnetic moment remains equal to zero and thus they should be classified as half-metallic fully compensated ferrimagnets, a class of materials very appealing for applications since the zero total spin moment means zero external stray magnetic fields and thus minimum energy losses. All alloys follow a generalized Slater-Pauling rule with the total spin magnetic moment per formula unit, M_t, inμ_B given in terms of the number of valence electrons per formula unit, Z_t, as $M_t = Z_t - (18 + 6 \times x)$, where x is the concentration of the extra Cr atoms in $Cr_{2+x}Se$. For Cr_3Se we have a small deviation from the Slater-Pauling rule for full-Heusler compounds ($x = 1$) since the antibonding single band created by the 4*s* states of the Cr and Se atoms in the spin-down band structure crosses the Fermi level due to the energy position of the latter states with respect to the 3*d* states of the Cr atoms.

The *d* orbitals of the Cr atoms reflect the different structures. In the case of Cr_2Se all atoms sit at sites of tetrahedral symmetry, while in Cr_3Se the two Cr atoms at the A and C sites (see Fig. 1) create a sublattice of octahedral symmetry. This behavior is also present as we compress the lattice. In the case of Cr_2Se all Cr atoms have localized spin-magnetic moments and upon compression of the lattice large values of them survive. In the case of Cr_3Se the Cr atoms at the A and C sites present spin magnetic moments of strong itinerant character while the Cr atoms at the B sites present localized magnetic properties. This coexistence of itinerant and localized magnetism is obvious when we examine the spin-density plots. As we compress the lattice at a certain value of the lattice parameter, the magnetization shows a sudden

jump, which is referred to as metamagnetism in the literature and has been observed in several Heusler compounds. If the lattice is further compressed, the increased hybridization of the *d* orbitals of the Cr atoms at the A and C sites completely kills their spin magnetic moments while the Cr atom at the B site keep a large portion of its spin magnetic moment.

Finally, calculations based on the frozen-magnon approximation revealed the complexity of the exchange interactions between the Cr atoms. The strong intersublattice antiferromagnetic coupling between the nearest-neighboring atoms stabilizes the ferrimagnetic character of both Cr_2Se and Cr_3Se and as a result the estimated Curie temperature within the mean field approximations is as high as 2524 K and 692 K, respectively. Both values exceed by far the room temperature and combined with the half-metallic antiferromagnetism make the $Cr_{2+x}Se$ alloys ideal for realistic spintronics applications.

*galanakis@upatras.gr
†kozdogan@yildiz.edu.tr
‡e.sasioglu@fz-juelich.de

[1] W. E. Pickett and J. S. Moodera, Phys. Today **54**(5), 39 (2001).
[2] M. I. Katsnelson, V. Yu. Irkhin, L. Chioncel, A. I. Lichtenstein, and R. A. de Groot, Rev. Mod. Phys. **80**, 315 (2008).
[3] P. J. Webster and K. R. A. Ziebeck, in *Alloys and Compounds of d-Elements with Main Group Elements*, Part 2, edited by H. R. J. Wijn, Landolt-Börnstein, New Series, Group III, Vol. 19, Pt. C (Springer-Verlag, Berlin, 1988), pp. 75–184.
[4] K. R. A. Ziebeck and K.-U. Neumann, in *Magnetic Properties of Metals*, edited by H. R. J. Wijn, Landolt-Börnstein, New Series, Group III, Vol. 32/C (Springer, Berlin, 2001), pp. 64–414.
[5] I. Galanakis, P. H. Dederichs, and N. Papanikolaou, Phys. Rev. B **66**, 134428 (2002).
[6] I. Galanakis, P. H. Dederichs, and N. Papanikolaou, Phys. Rev. B **66**, 174429 (2002).
[7] X. Hu, Adv. Mater. **24**, 294 (2012).
[8] S. Wurmehl, H. C. Kandpal, G. H. Fecher, and C. Felser, J. Phys.: Condens. Matter **18**, 6171 (2006).
[9] H. van Leuken and R. A. de Groot, Phys. Rev. Lett. **74**, 1171 (1995).
[10] M. Shaughnessy, C. Y. Fong, L. H. Yang, and C. Felser, arXiv:1108.3651.
[11] E. Şaşıoğlu, Phys. Rev. B **79**, 100406(R) (2009).
[12] B. Balke, G. H. Fecher, J. Winterlik, and C. Felser, Appl. Phys. Lett. **90**, 152504 (2007).
[13] J. Winterlik, B. Balke, G. H. Fecher, C. Felser, M. C. M. Alves, F. Bernardi, and J. Morais, Phys. Rev. B **77**, 054406 (2008).
[14] I. Galanakis, K. Özdoğan, E. Şaşıoğlu, and B. Aktaş, Phys. Rev. B **75**, 172405 (2007).
[15] K. Özdoğan and I. Galanakis, J. Magn. Magn Mater. **321**, L34 (2009).
[16] I. Galanakis, K. Özdoğan, E. Şaşıoğlu, and B. Aktaş, Phys. Status Solidi A **205**, 1036 (2008).
[17] I. Galanakis, K. Özdoğan, E. Şaşıoğlu, and B. Aktaş, Phys. Rev. B **75**, 092407 (2007).
[18] H. Luo, L. Ma, Z. Zhu, G. Wu, H. Liu, J. Qu, and Y. Li, Physica B **403**, 1797 (2008).
[19] W. E. Pickett, Phys. Rev. B **57**, 10613 (1998).
[20] J. H. Park, S. K. Kwon, and B. I. Min, Phys. Rev. B **65**, 174401 (2002).
[21] M. Uehara, M. Yamada, and Y. Kimishima, Solid State Commun. **129**, 385 (2004).
[22] Y. K. Wang and G. Y. Guo, Phys. Rev. B **73**, 064424 (2006).
[23] V. Pardo and W. E. Pickett, Phys. Rev. B **80**, 054415 (2009).
[24] M. Nakao, Phys. Rev. B **74**, 172404 (2006).
[25] M. Nakao, Phys. Rev. B **77**, 134414 (2008).
[26] H. Akai and M. Ogura, Phys. Rev. Lett. **97**, 026401 (2006).
[27] N. H. Long, M. Ogura, and H. Akai, J. Phys.: Condens. Matter **21**, 064241 (2009).
[28] M. Nakao, Phys. Rev. B **83**, 214404 (2011).
[29] S. Picozzi, A. Continenza, and A. J. Freeman, Phys. Rev. B **69**, 094423 (2004).
[30] J. Winterlik, B. Balke, G. H. Fecher, C. Felser, M. C. M. Alves, F. Bernardi, and J. Morais, Phys. Rev. B **77**, 054406 (2008).
[31] H. Kurt, K. Rode, M. Venkatesan, P. Stamenov, and J. M. D. Coey, Phys. Rev. B **83**, 020405(R) (2011).
[32] H. Kurt, K. Rode, M. Venkatesan, P. Stamenov, and J. M. D. Coey, Phys. Status Solidi B **248**, 2338 (2011).
[33] J. Li, H. Chen, Y. Li, Y. Xiao, and Z. Li, J. Appl. Phys. **105**, 083717 (2009).
[34] Q. F. Li, C. H. Yang, and J. L. Su, Physica B **406**, 3726 (2011).
[35] I. Galanakis and E. Şaşıoğlu, Appl. Phys. Lett. **99**, 052509 (2011).
[36] J. Rusz, L. Bergqvist, J. Kudrnovsky, and I. Turek, Phys. Rev. B **73**, 214412 (2006).
[37] H. M. Huang, S. J. Luoa, and K. L. Yao, Physica B **406**, 1368 (2011).
[38] P. J. Webster and R. M. Manikinar, J. Magn. Magn. Mater. **42**, 300 (1984).
[39] K. Koepernik and H. Eschrig, Phys. Rev. B **59**, 1743 (1999).
[40] J. P. Perdew, K. Burke, and M. Ernzerhof, Phys. Rev. Lett. **77**, 3865 (1996).
[41] A. R. Williams, J. Kübler, and C. D. Gelatt, Phys. Rev. B **19**, 6094 (1979).
[42] O. K. Andersen, Phys. Rev. B **12**, 3060 (1975).
[43] L. M. Sandratskii and P. Bruno, Phys. Rev. B **66**, 134435 (2002).
[44] I. Galanakis, Ph. Mavropoulos, and P. H. Dederichs, J. Phys. D: Appl. Phys. **39**, 765 (2006).
[45] D. Jiles, *Introduction to Magnetism and Magnetic Materials* (Chapman & Hall, London, 1998).
[46] E. Şaşıoğlu, L. M. Sandratskii, and P. Bruno, J. Phys.: Condens. Matter **17**, 995 (2005); K. Özdoğan, I. Galanakis, E. Şaşıoğlu, and B. Aktas, *ibid.* **18**, 2905 (2006); G. D. Liu, X. F. Dai, H. Y. Liu, J. L. Chen, Y. X. Li, Gang Xiao, and G. H. Wu, Phys. Rev. B **77**, 014424 (2008).
[47] I. Galanakis and E. Şaşıoğlu, Appl. Phys. Lett. **99**, 052509 (2011).
[48] I. Galanakis and E. Şaşıoğlu, Appl. Phys. Lett. **98**, 102514 (2011).
[49] J. Y. Rhee and B. N. Harmon, Phys. Rev. B **70**, 094411 (2004).
[50] E. Şaşıoğlu, L. M. Sandratskii, and P. Bruno, Phys. Rev. B **71**, 214412 (2005).
[51] M. Meinert, J.-M. Schmalhorst, C. Klewe, G. Reiss, E. Arenholz, T. Böhnert, and K. Nielsch, Phys. Rev. B **84**, 132405 (2011).
[52] E. Şaşıoğlu, L. M. Sandratskii, P. Bruno, and I. Galanakis, Phys. Rev. B **72**, 184415 (2005).

[53]E. Şaşıoğlu, L. M. Sandratskii, and P. Bruno, Phys. Rev. B **77**, 064417 (2008); Appl. Phys. Lett. **89**, 222508 (2006).
[54]K. Sato, L. Bergqvist, J. Kudrnovský, P. H. Dederichs, O. Eriksson, I. Turek, B. Sanyal, G. Bouzerar, H. Katayama-Yoshida, V. A. Dinh, T. Fukushima, H. Kizaki, and R. Zeller, Rev. Mod. Phys. **82**, 1633 (2010).
[55]Y. Kurtulus, R. Dronskowski, G. D. Samolyuk, and V. P. Antropov, Phys. Rev. B **71**, 014425 (2005).
[56]J.-M. Schmalhorst, G. Reiss, and M. Meinert, J. Phys.: Condens. Matter **23**, 116005 (2011).
[57]M. Meinert, J.-M. Schmalhorst, and G. Reiss, J. Phys.: Condens. Matter **23**, 036001 (2011).
[58]I. Galanakis, E. Şaşıoğlu, and K. Özdoğan, Phys. Rev. B **77**, 214417 (2008); J. Kudrnovský, V. Drchal, I. Turek, and P. Weinberger, *ibid.* **78**, 054441 (2008); I. Galanakis and E. Şaşıoğlu, J. Appl. Phys. **109**, 113912 (2011).
[59]K. Özdoğan, E. Şaşıoğlu, and I. Galanakis, J. Phys. D: Appl. Phys. **42**, 085003 (2009).
[60]S. K. Ren, W. Q. Zou, J. Gao, X. L. Jiang, F. M. Zhang, and Y. W. Du, J. Magn. Magn. Mater. **288**, 276 (2005).
[61]C. Walle, L. Offernes, and A. Kjekshus, J. Alloys Compounds **349**, 105 (2003).
[62]J. Rusz, I. Turek, and M. Diviš, Phys. Rev. B **71**, 174408 (2005).
[63]J. Kübler, Phys. Rev. B **67**, 220403 (2003).